Environmental Science and Pollution Research (2024) 31:50709–50721
https://doi.org/10.1007/s11356-024-34559-1

RESEARCH ARTICLE

Utilization of industrial wastes in non-sintered bricks: microstructure and environmental impacts

Daquan Shi[1] · Xiaobing Ma[1] · Yading Zhao[1] · Jian Wang[1] · Yan Xia[1,2] · Minghao Liu[1,3]

Received: 8 January 2024 / Accepted: 26 July 2024 / Published online: 5 August 2024

Abstract
Recycling industrial solid wastes as building materials in the construction field exhibits great environmental benefits. This study designed an eco-friendly non-sintered brick by combining multiple industrial solid wastes, including sewage sludge, fly ash, and phosphorus gypsum. The mechanical properties, microstructure, and environmental impacts of waste-based non-sintered bricks (WNBs) were investigated comprehensively. The results revealed that WNB exhibited excellent mechanical properties. In addition, steam curing could further promote the strength development of WNB. The compressive strength of WNB with 10 wt% of sewage sludge reached 13.5 MPa. Phase assemblage results indicated that the incorporation of sewage sludge promoted the generation of ettringite. Mercury intrusion porosimetry results demonstrated that the pore structure of WNB varies with the dosage of sewage sludge. Life-cycle assessment results revealed that the energy consumption and CO_2 emission of WNB were 45% and 17% lower than those of traditional clay bricks. Overall, the development of WNB in this study provided insights into the co-disposal of industrial solid wastes.

Keywords Industrial solid waste · Sewage sludge · Wasted-based non-sintered bricks · Environmental benefits · Mechanical properties · Life-cycle assessment

Introduction

With the rapid progress of urbanization, a large number of industrial solid wastes have been produced (Wang et al. 2022, 2020, 2023; Xu et al. 2023). Industrial solid wastes usually occupy abundant land resources and pollute water, soil, and air, which is harmful to humans (Mendes et al. 2019; Wang et al. 2024a, 2024e; Yao et al. 2024). In addition, mining natural sand also has shortcomings, such as resource shortage and environmental pollution. The utilization of industrial solid waste-based building materials is regarded as a promising disposal method, which saves natural building materials and realizes the resource recovery of industrial solid wastes (He et al. 2023; Wang et al. 2024d; Xia et al. 2024). Industrial solid wastes, sewage sludge (SS), fly ash (FA), and phosphorus gypsum (PG) have garnered increasing attention recently. SS is produced as a waste product after undergoing mechanical, biological, and chemical treatment processes in sewage treatment facilities (Cwiertniewicz-Wojciechowska et al. 2023; Liu et al. 2023; Xia et al. 2023a). FA and PG are generated in significant quantities by the industrial processes of coal combustion in power plants and the production of phosphoric acid in the fertilizer industry, respectively.

The increasing urbanization has resulted in a significant increase in the generation of SS, with China producing approximately 40 million tons annually. It is urgent to solve the problem of SS disposal. Notably, the composition of SS is very complex. More than half of the compounds in SS are harmful substances, for instance, heavy metals and pathogenic organisms, which will cause irreversible damage to the bloodstream, nervous system, and organs (Riaz et al. 2020; Zhou et al. 2023). If not properly managed, SS will cause serious environmental problems, such as water pollution and soil contamination (Sigua and Adjei 2005, Xia et al. 2022).

Responsible Editor: Philippe Garrigues

✉ Yading Zhao
zhaoyd@hit.edu.cn

1 School of Civil Engineering, Harbin Institute of Technology, Harbin 150090, China

2 State Key Laboratory of Clean Energy Utilization, Zhejiang University, Hangzhou 310027, China

3 Tianjin Cement Industry Design and Research Institute Co., Ltd., Tianjin 300131, China

The SS removing water through sewage plants is stable and odorless. This simplifies the subsequent treatment steps for SS. However, due to economic constraints, the subsequent treatment steps of sewage sludge are limited to landfill and deposition inside waste pits (Lu et al. 2017). Interestingly, due to the presence of SiO_2, Fe_2O_3, and Al_2O_3, SS has the potential for building material utilization (Dang et al. 2023; Ma et al. 2024; Xia et al. 2023b). Previous research has shown that sewage sludge ash can partially replace cement in concrete production due to its pozzolanic activity (Baeza et al. 2014). This is attributed to the fact that the mineral composition of SS after high-temperature-treatment is similar to that of cement clinker (Chikouche et al. 2016; Ma et al. 2023). However, the thermal treatment of SS consumes a substantial amount of energy and contributes to increased carbon dioxide emissions, diminishing its environmental advantages. Therefore, dried SS is considered more suitable as a building material than sewage sludge ash. FA is also used as a supplement cementitious material in concrete production due to its unique components. However, the FA generation in China in 2019 alone reached 540 million tons and accounted for 39.13% of general industrial solid waste, leading to substantial FA accumulation (Hou et al. 2023; Jitchaiyaphum et al. 2013; Zhang et al. 2022a), although over 70 million tons of PG are produced by the phosphate fertilizer industry in China. However, due to strong acidity and complex impurity, less than 15% of PG can be reused in agriculture, sulfuric acid production, cement production, building materials, and soil stabilization (Ding et al. 2019). The accumulation of SS, FA, and PG essentially occupies land resources. This poses significant environmental challenges due to the potential of sewage sludge, FA, and PG to leach contaminants into the surrounding soil, atmosphere, and groundwater (Zhang et al. 2022a).

As a building material widely used in brick-paved roads, clay bricks consume large amounts of non-renewable clay resources from arable land. The usage of clay bricks as a traditional building material is facing limitations due to the scarcity of arable land resources in China (such as roadbeds) (Cheng et al. 2021; Yague et al. 2005). To minimize the production of clay bricks, using wastes in place of natural clay for manufacturing sintered bricks has significantly achieved both harmlessness and resource utilization (Wu et al. 2022a). However, the sintering process for clay bricks consumes vast energy and increases carbon emissions (Shaik et al. 2022). In addition, the collaborative disposal of multiple industrial solid wastes has great prospects for the application of building materials. This is regarded as an excellent industrial solid waste treatment method.

Therefore, this study investigates the feasibility of recycling multiple industrial solid wastes into non-sintered bricks. The developed waste-based non-sintered bricks (WNBs) were composed of SS, FA, PG, and quicklime. The macro-properties of WNB, including mechanism strength, bulk density, and water absorption, were investigated. In addition, the phase assemblage and microstructure of WNB were evaluated via X-ray diffraction (XRD) and scanning electron microscopy (SEM). The pore structure of WNB was conducted using mercury intrusion porosimetry (MIP). Furthermore, the leaching behavior of potentially toxic elements (PTEs) in WNB was evaluated based on the toxicity characteristic leaching procedure (TCLP). The environmental impacts of WNB were determined by life cycle assessment (LCA) and compared with the traditional clay bricks.

Materials and methods

Materials

The SS was collected from Longjiang Environmental Protection Group Co. Ltd. in Harbin, China. The thermal behavior of the raw sewage sludge is shown in Fig. S1. The results indicated that the decomposition of organic matter in SS was mainly at 292.2 °C. Thereby, the raw SS was dried in a muffle furnace at 300 °C for 2 h to decompose organic matter and then broke into small pieces, avoiding energy consumption and the release of a large number of harmful gases (volatile organic compounds, ammonia, and polycyclic aromatic hydrocarbons) caused by the high-temperature calcination process of sludge (Peng et al. 2016; Xia et al. 2023e). Table S1 shows the chemical compositions of the SS, which mainly contains SiO_2, Fe_2O_3, and Al_2O_3. The morphology, XRD pattern, and Fourier transform infrared (FT-IR) pattern of sewage sludge are shown in Fig. S2, S3, and S4, respectively. The main mineral phases in sewage sludge included quartz and hematite. Absorption bands of FT-IR (777.18 cm^{-1}, 3120.25 cm^{-1}, and 470.54 cm^{-1}) further demonstrated the presence of SiO_2, Al_2O_3, and Fe_2O_3 in SS. The quicklime used in this study was manufactured by Hangzhou Haituo Calcium Industry Co. Ltd. in China. The FA was sourced from a thermal power plant in Harbin, China, and the PG was produced by Guizhou Wengfu Group in China.

Preparation of WNB

In the WNB, quicklime was added as an alkali-activator. It increased the pH of the mixture, facilitating the dissolution of sulfates and aluminosilicates. FA provided aluminosilicates, which were crucial for forming C-(A)-S–H gels during hydration. PG was added as a sulfate activator, which could react with aluminates to form ettringite under the action of the alkali-activator. The high-temperature conditions in the preparation process accelerated the dissolution of aluminosilicates and sulfates and the formation of ettringite, shortening the curing age and improving the mechanical strength of WNB. Besides, dried sludge was crushed as aggregate to avoid energy consumption during grinding.

The mixture proportions of the twelve groups of WNB are listed in Table 1. The dosage of PG was fixed at 3 wt%, and the water-to-binder ratio was maintained at 1:1.2 in all mixtures. The dosage of quicklime varied from 10 wt% to 15 wt% and 20 wt%. Additionally, SS was used as aggregate and partially replaced the river sand at 0, 10 wt%, 20 wt%, and 30 wt%. The ratio of binder materials to aggregates in WNB was 1:0.67.

For the preparation of WNB, the corresponding weight of binder materials was blended with river sand and SS for 2 min to ensure a homogeneous distribution (Xia et al. 2023d). Subsequently, water was slowly added and blended for another 3 min. The fresh specimens were poured into steel models (40 × 40 × 160 mm^3) and vibrated 60 times to remove bubbles (Shi et al. 2024b; Wang et al. 2024c). After that, the specimens were covered with polyethylene films and pre-cured for 24 h at room temperature. The hardened samples were demolded after pre-curing and transferred into steam curing boxes with different temperatures (50 °C, 70 °C, and 90 °C) to explore the most suitable accelerated curing condition of WNB. The preparation of samples for microanalysis was performed as follows (Yu et al. 2024a; Zhu et al. 2024b): (i) specimens were cut into small pieces after steam curing for 1 day and 3 days; (ii) broken samples were immersed in isopropanol for 7 days to stop reaction; (iii) the samples were dried at 40 °C for another 3 days.

Test and characterization

The compressive strength and flexural strength of WNB with different mixture proportions and curing temperatures were measured with a loading rate of 1.0 kN/s (Zhu et al. 2024a). The bulk density and water absorption test of the specimen were carried out according to GB/T2542-2012. The samples were placed in a blast drying oven at 105 °C and dried to constant weight. Measure the length of the three sides of WNB with a micrometer. To calculate the volume of the specimen, the length, width, and height were measured twice in the middle of the two surfaces of WNB, respectively. The bulk density ρ was calculated according to Eq. (1). The water absorption rate was determined by the difference of weight after soaking the WNB in 20 °C water for 24 h, calculated according to Eq. (2).

$$\rho = \frac{m}{V} \tag{1}$$

where m and V represent the weight and volume of samples, respectively.

$$W_{24} = \frac{M_{24} - M_0}{M_0} \times 100\% \tag{2}$$

where W_{24} represents the water absorption rate of WNB after soaking in 20 °C water for 24 h, and M_0 and M_{24} represent the weight of WNB before and after soaking in water for 24 h, respectively.

The mineral compositions of WNB were determined by XRD analysis, which was conducted using the Rigaku Smartlab 9-kW instrument operating at 40 kV and 40 mA. The scanning range was 5° to 60° 2θ, and the step size was 0.0135° 2θ (Wang et al. 2024b). The morphology of hydration products in hardened WNB was detected by SEM (TESCAN) under the secondary electron mode with a voltage of 30 kV (Yu et al. 2024b). The pore structure parameters of the hardened mortar samples were determined via MIP (IV 9500) with a maximum pressure of 228 MPa (Shi et al. 2024a). The leaching behavior of heavy metals in hardened WNB was determined by TCLP. LCA of WNB aimed to evaluate its environmental impacts, specifically examining

Table 1 Mixture proportions of WNB (%)

Samples	Quicklime	Fly ash	Phosphorus gypsum	Sewage sludge	Sand	Water
Q10S0	10	47	3	0	40	50
Q10S1	10	47	3	10	30	50
Q10S2	10	47	3	20	20	50
Q10S3	10	47	3	30	10	50
Q15S0	15	42	3	0	40	50
Q15S1	15	42	3	10	30	50
Q15S2	15	42	3	20	20	50
Q15S3	15	42	3	30	10	50
Q20S0	20	37	3	0	40	50
Q20S1	20	37	3	10	30	50
Q20S2	20	37	3	20	20	50
Q20S3	20	37	3	30	10	50

global warming potential (GWP), fossil fuel depletion (FFD), acidification potential (AP), and photochemical ozone creation potential (POCP) (Mulya et al. 2022). The LCA model was built through the SimaPro software, focusing on the “from cradle to gate” stage, and its system boundary was illustrated in Fig. S5 (Xia et al. 2023c). The life cycle inventory (LCI) data were sourced from the Ecoinvent 3.1 database, supplemented by previous studies (Capony et al. 2013; Cuenca-Moyano et al. 2019, Gupta and Kua 2020).

Results and discussion

Physical properties

The mixture proportions of WNB significantly influenced its physical properties. The 1-day and 3-day compressive strength and flexural strength of WNB under different curing temperatures are shown in Fig. 1. It could be observed that both the compressive strengths and flexural strength of WNB decreased with the increase in the dosage of SS. This indicated that the incorporation of SS exhibited an adverse impact on the strength development of WNB. This could be attributed to the porous characteristics of SS, as well as its lower hardness as a substituted aggregate. Both of them result in a deterioration of mechanical properties. However, compressive and flexural strengths increased in some intervals with the increasing SS dosage. This phenomenon was because the activity component in sludge was dissolved to form additional hydration products, offsetting the above adverse effects. With the increase in the quicklime dosage, the compressive strength and flexural strength of WNB increased first and then decreased. WNB with 15 wt% of quicklime exhibited the best mechanical properties. This can be attributed to the balance between calcareous materials and siliceous materials. The absence of quicklime contributed to a deficiency in calcareous raw materials, thereby hindering the generation of hydration products (Gnisci 2022; Wu et al. 2022b). Conversely, an excessive dosage of quicklime resulted in insufficient siliceous raw materials. Moreover, the strength development of WNB was also influenced by the curing temperature and curing ages. Generally, with the increase in the curing temperature and age, the mechanical properties of specimens are enhanced due to the compact microstructure and substantial C-S–H gels (Balendran and Martin-Buades 2000, Chen 2021). Higher curing temperatures promoted the dissolution of reactants and the precipitation of hydration products. Thus, under a high curing temperature, the matrix of WNB specimens was filled with more hydration products, promoting its strength development. It could be observed that under conditions at 70 °C for 3 days and 90 °C for 1 day, the compressive strength of WNB with 15 wt% quicklime and 20 wt% SS still maintained a level of 8 MPa. However, unevenly distributed hydration products caused by prolonged high-temperature curing might also contribute to the opposite phenomenon: the decrease in strength with increasing curing temperature and age in some intervals (Duan et al. 2022). Obviously, the compressive strength of WNB with 15 wt% quicklime and curing condition at 90 °C for 3 days was higher than WNB with other dosage of quicklime and steam curing regime, and the compressive strengths of WNB with 0, 10 wt%, 20 wt%, and 30 wt% sewage sludge were 23.4, 13.5, 6.8, and 4 MPa, respectively. Besides, curing at 90 °C for 3 days, the phase composition and microstructure of WNB develop sufficiently to be clearly observed. These four groups were selected to investigate variations in phase composition and microstructure. However, due to the compressive strength of WNB with 15 wt% quicklime and 30 wt% SS lower than 5 MPa, just WNBs with 0, 10 wt%, and 20 wt% SS were selected to perform pore structure and leaching behavior. Although the characteristics of waste materials hindered the strength development of WNB, the mechanical properties of WNB could be guaranteed based on the regulation of raw materials proportions and the activation of the steam curing regime.

The bulk densities of WNB with different dosages of SS are shown in Fig. 2a. Obviously, the bulk density of WNB decreased with the increase in the dosage of SS. This could be attributed to the low density of SS particles. In addition, the water absorption characteristic of WNB varied with the dosages of SS, as shown in Fig. 2b. Due to the irregular shape and large specific surface area of SS particles, the water absorption rate of WNB increased with the incorporation of SS (Zhang et al. 2022b). The water absorption rate of the WNB specimen with 20 wt% SS was close to 50%, which was 14% higher than that of SS-free WNB. In Fig. 2c, the strength retention of WNB after soaking in water for 24 h declined with the dosage of SS increase. This was associated with the increase in the porosity of the specimens. The porous characteristics and extremely weak pozzolanic activity of SS exhibited an adverse impact on the pore structure of WNB specimens. The high-water absorption rate of the WNB specimen could seriously affect its frost resistance.

Phase assemblage

The phase assemblage of WNB was associated with its mixture proportions. As shown in Fig. 3, the major mineral phases in WNB specimens included quartz, ettringite, hematite, limestone, and gypsum. During the reaction process of WNB, portlandite was generated first as the intermediate hydration product from the reaction of quicklime, as shown in Eq. (3). Subsequently, portlandite was consumed by the precipitation of C-S–H gels and

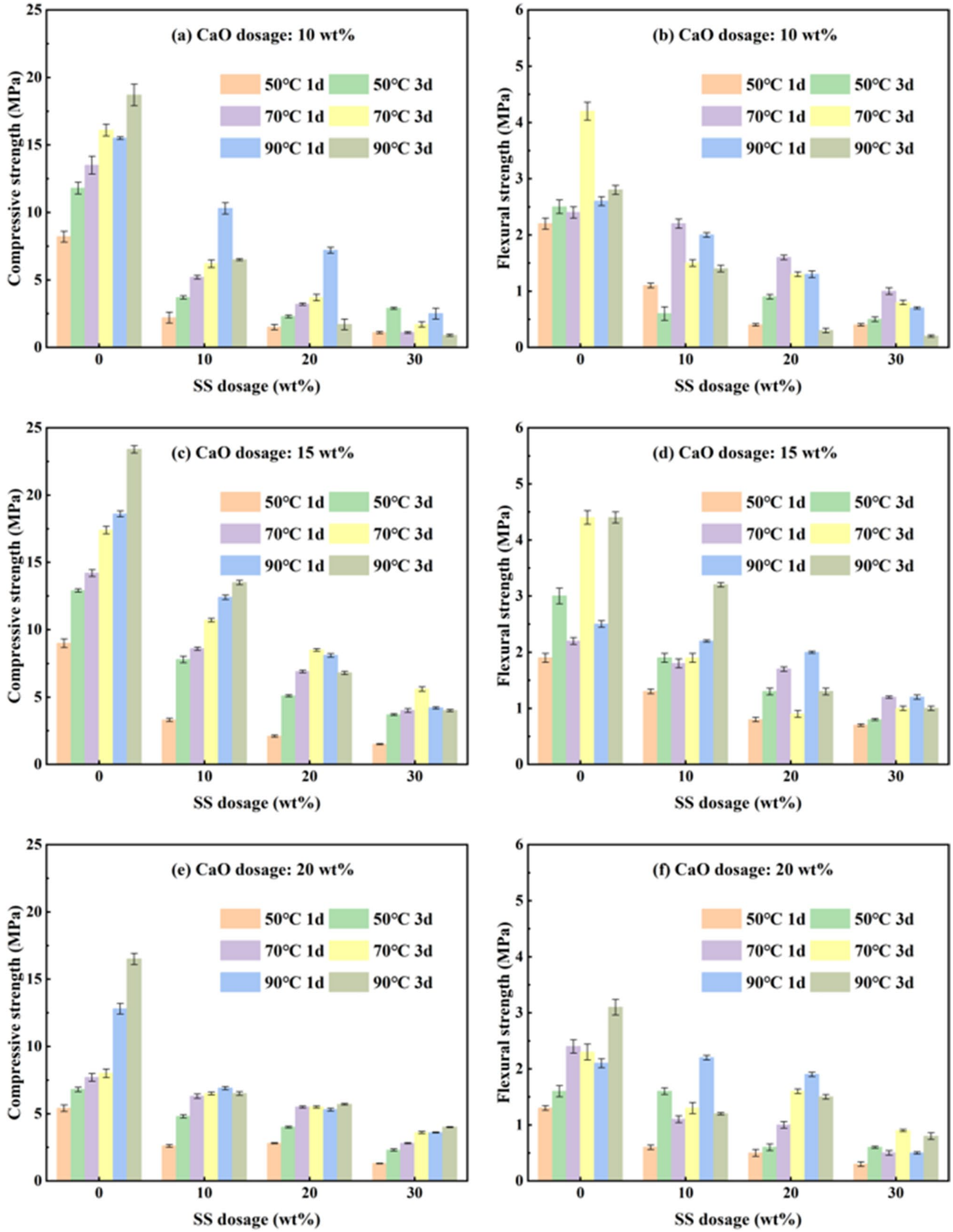

Fig. 1 Mechanical strength of WNB under different curing temperatures and ages

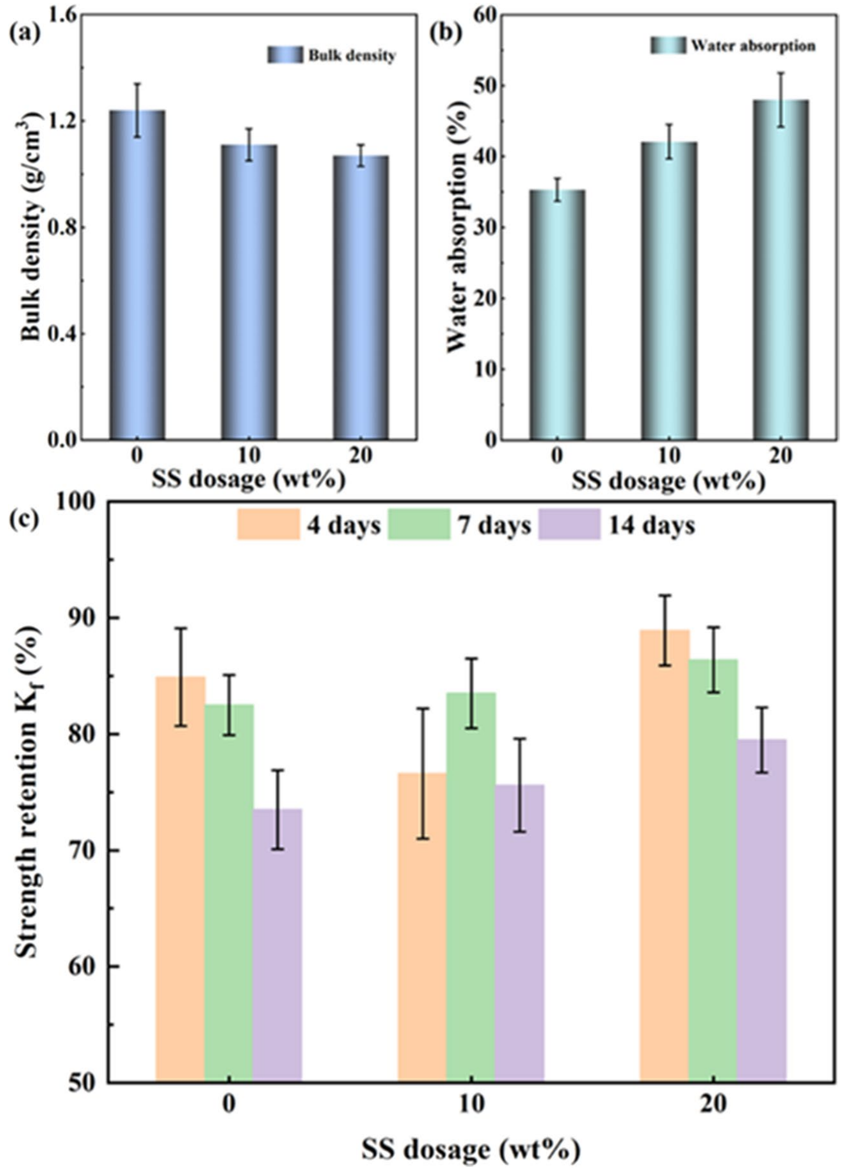

Fig. 2 Water resistance of WNB: **a** bulk density, **b** water absorption, and **c** strength retention

ettringite as shown in Eq. (4). It should be noticed that the incorporation of SS promoted the generation of ettringite in WNB. This was because aluminates and ferrite were the most soluble elements in SS, and these phases could be captured by sulfates with the generation of ettringite.

$$CaO + H_2O \rightarrow Ca(OH)_2 \quad (3)$$

$$AS_2 + 6.4Ca(OH)_2 + 3CaSO_4 \bullet 2H_2O + 33.6H_2O \rightarrow 2C_{1.7}SH_4 + C_6A\hat{s}_3H_{32} \quad (4)$$

where AS_2 represents the active aluminosilicates in FA and SS, and $C_6A\hat{s}_3H_{32}$ represents the ettringite.

Micromorphology

The micromorphology of WNB was influenced by its mixture proportions. As shown in Fig. 4a–d, with the increase in the addition level of SS, the matrix of WNB was looser and filled with fewer hydration products. This could be attributed to the porous structure and weak pozzolanic reactivity of SS. This was consistent with the compressive strength results, which showed that the compressive strengths of WNB decreased with the increase in the addition level of SS. In addition, although the differences in compactness

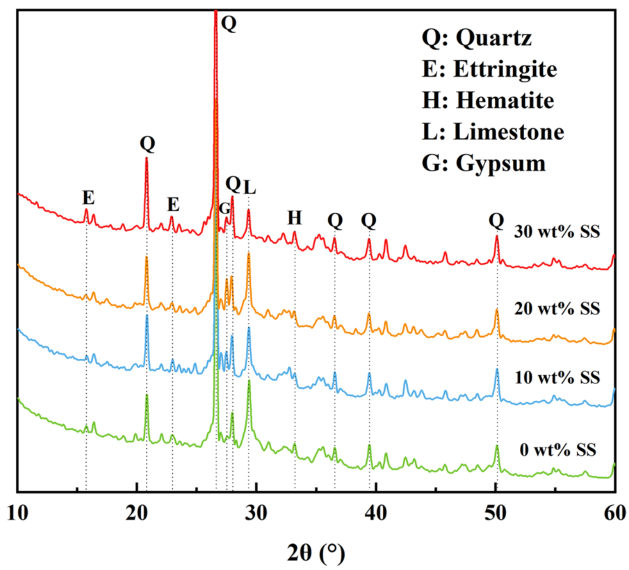

Fig. 3 Phase assemblage of WNB with various sewage sludge content

between different samples are relatively small, the presence of sewage sludge particles is quite pronounced (Fig. 4e–h). C-S–H gels were the major hydration products, and their generation greatly influenced the strength development of WNB. However, it is well known that C-S–H gels are amorphous, and it is not easy to characterize their content quantitatively. Therefore, the relative content of C-S–H gels was reflected based on the coating situation of fly ash particles. Obviously, in sewage SS-free WNB, the FA particle was tightly surrounded by hydration products, while in sewage SS-contained WNB, the FA particle was coated with plenty of unreacted and porous sludge particles. This further revealed that the incorporation of SS inhibited the generation of hydration products, especially C-S–H gels. It was attributed to the minor elements and orthophosphate ions (PO_4^{3-}) in SS (Cyr et al. 2007; Mejdi et al. 2020). Moreover, the micromorphology of ettringite in WNB varied with the additional level of SS, as shown in Fig. 4i–m. In SS-free WNB, the needle-like ettringite was distributed in the pore of the matrix. Thus, the matrix of Q15S0 was majorly filled with C-S–H and refined with ettringite, leading to an excellent mechanical property. With the incorporation of SS, more ettringite was generated on the surface of SS particles due to the dissolution of aluminates and ferrites from SS. Besides, it should be noted that the crystal size of ettringite sharply increased with the addition of SS. In Q15S3, the large and coarse ettringite was distributed on the surface of C-S–H, which could not exhibit the refinement effect on the pore structure of WNB.

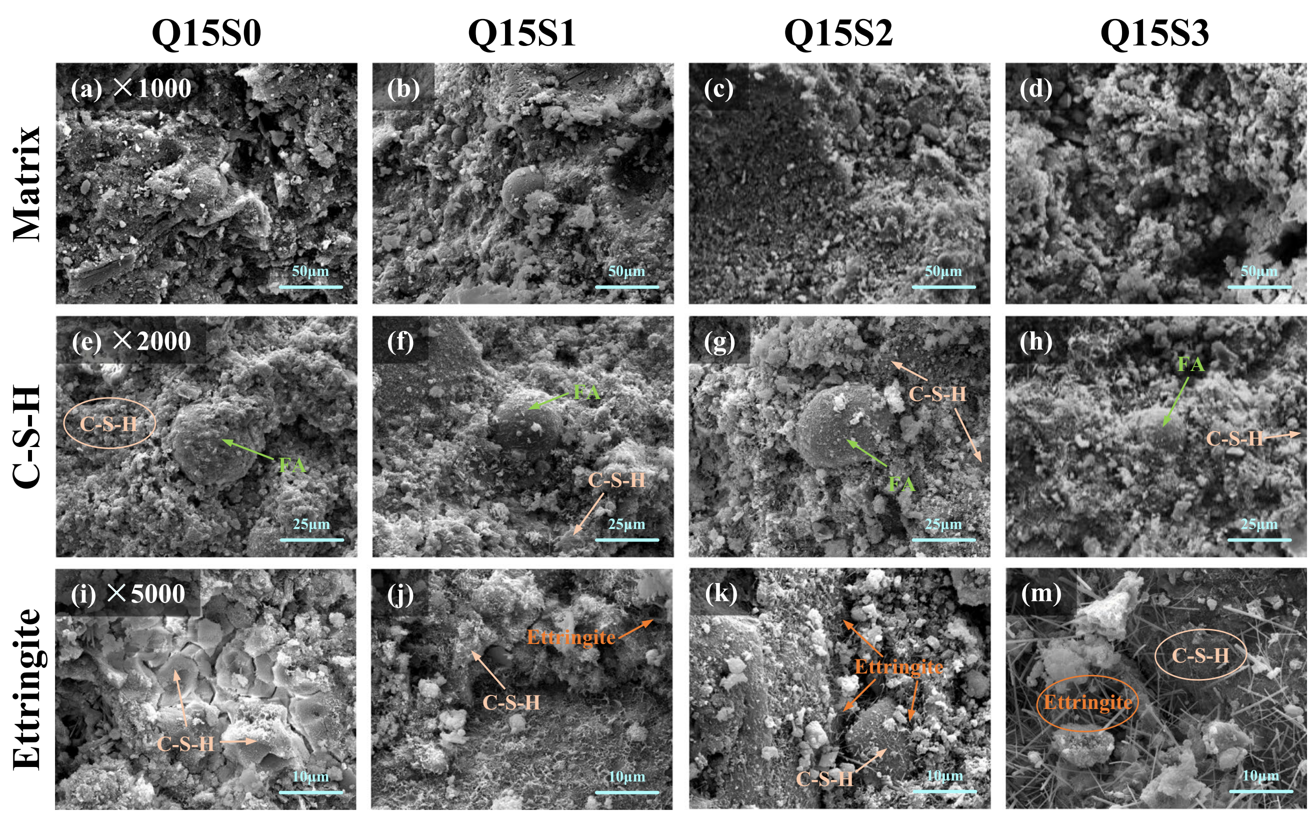

Fig. 4 SEM images of WNB with various sewage sludge content

Pore structure

The pore structure of WNB is shown in Fig. 5. It could be observed that the cumulative pore volume of WNB increased with the increase in the dosage of SS. This indicated that the addition of SS resulted in the deterioration of the pore structure of WNB. This could be associated with the porous characteristics of SS. It is well known that the mechanical properties of building materials were associated with pore volume. The mechanical properties increased with the increase of total pore volume. This was consistent with the result that the compressive strengths of WNB decreased while its cumulative pore volume increased. The critical pore size of specimens is the inflexion on the cumulative pore volume curve, representing the maximum pore size corresponding to a significant increase in the volume of intrusion mercury. Figure 5a also showed that the critical pore size of SS-contained WNB was over 0.1 μm, while the critical pore size of SS-free WNB was only 0.03 μm. This indicated that the critical pore diameter increased with the incorporation of SS, which increased the pore connectivity of WNB (Lyu et al. 2020). The deterioration of the pore structure was in accordance with the results that the water absorption rate of WNB increased with the incorporation of SS. To more comprehensively evaluate the effect of SS incorporation on the pore structure of WNB, the pores of WNB were divided into three zones based on pore diameter ranges (Fig. 5b). Pore sizes of 10 ~ 1000 μm, 0.1 ~ 10 μm, and less than 0.1 μm were defined as air pores, mesopores, and capillary pores, respectively (Wang et al. 2021). With the increase in the incorporation level of SS, the relative content of mesopores increased, and the relative content of capillary pores decreased. Enlarging pore size could result in the lower mechanical properties of paste specimens.

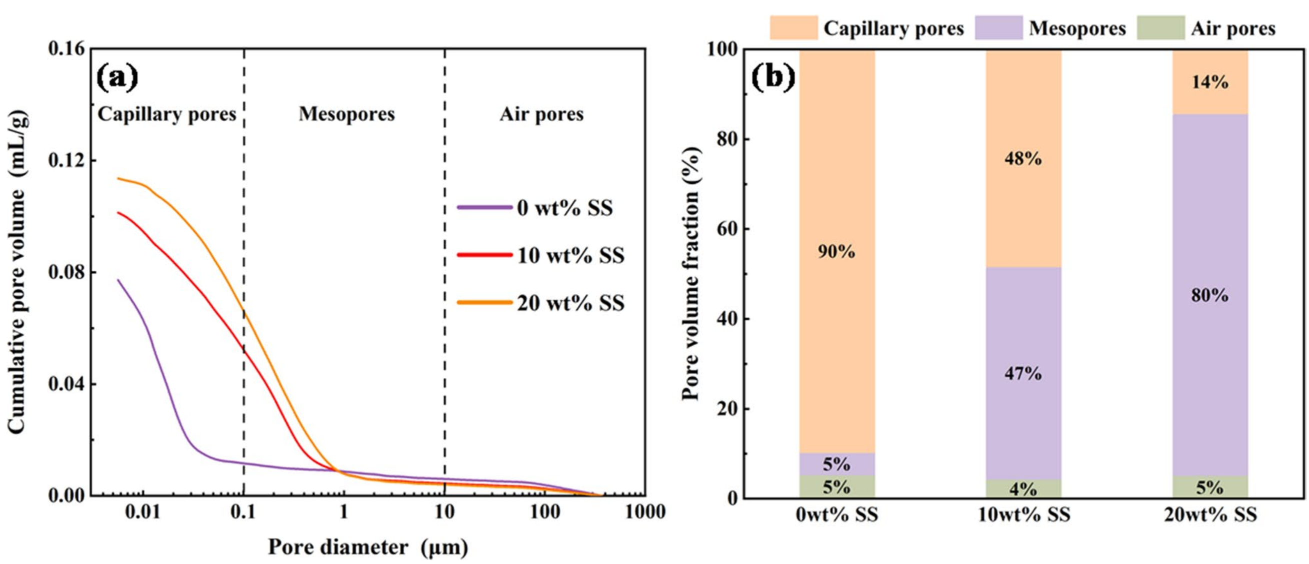

Fig. 5 Pore structure of WNB with various sewage sludge content

Leaching behavior

The leaching behavior of PTEs in the matrix of WNB is shown in Fig. 6. With the increase in the additional level of SS, the concentration of PTEs in the leachate of WNB was increased. The leaching concentration of Cr and Pb was 0.046 and 0.009 mg/L, respectively. The leaching behavior of PTEs in all specimens complied with the requirements of construction materials based on the Chinese standard of GB 18599–2020. This indicated that the PTEs were stabilized in the matrix of WNB, and the

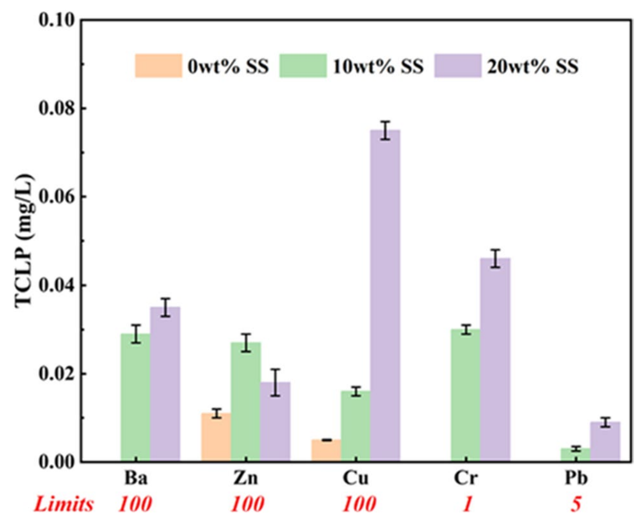

Fig. 6 Leaching behavior of PTEs in the matrix of WNB

developed WNB could be safely used as pavement materials. The excellent immobilization effect of WNB on the PTEs could be attributed to the following reasons. PTEs mainly existed in organic matter, sulfide, oxide, hydrate, and other elements of SS. The desiccation of SS was accompanied by the decomposing of organic. The reduction of organic content in SS made PTEs combine with inert residues. The conversion of SS from active to inert weakened the migration ability of heavy metals (Chen et al. 2021). Besides, when SS was mixed with quicklime, the acid-soluble heavy metals in SS transformed. The diffusion ability of acid-solution heavy metals was reduced (Yuan et al. 2011). In addition, the migration of heavy metals during the curing process of WNB specimens was relatively complex. The heavy metals may be adsorbed onto the surface of the C-S–H gels in the form of ions or reacted with other elements, resulting in the heavy metals being effectively consolidated in the matrix of WNB (Cui et al. 2022; Liu et al. 2022a, 2022b). Moreover, the matrix structure of WNB could further inhibit the leaching behavior of PTEs due to its physical coating effect.

Environmental impacts

LCA was conducted to evaluate the environmental impacts of WNB, including FFD and GWP, as shown in Fig. 7. It was observed that the FFD and GWP values of SS were negative. This was attributed to the avoidance of environmental impacts associated with the conventional treatment of sewage sludge (Huang et al. 2023). The FFD and GWP values of WNB decreased with the increase in the incorporation level of SS. FFD and GWP values of Q15S3 were 1.806 MJ/kg and 0.230 kg CO_2/kg, respectively. This was posed by reducing environmental impacts by avoiding landfills and incineration (Septien et al. 2020). Furthermore, the environmental impacts contributed by quicklime were significant in WNB; the FFD and GWP values of quicklime were far higher than those of other binder materials. Under the exact content of SS, the FFD and GWP values of WNB escalated with the increase in the addition level of quicklime. This was attributed to FA and PG being industrial solid wastes, and recycling them as binder materials in WNB exhibited great environmental benefits. In addition, both raw materials and the mixing process were taken into consideration for environmental impacts. It was observed that the environmental impacts during the mixing process were significantly smaller compared to raw materials. This could be attributed to that the production of raw materials required high-power mechanical to process.

In order to comprehensively evaluate the influences of SS incorporation on the environmental impacts and mechanical properties of WNB, the original results of LCA were normalized according to the compressive strength of WNB after curing for 1 day at 90 ℃ or 3 days at 90℃. Compressive strength is considered an essential parameter in construction materials (Proske et al. 2018). The normalized results of LCA were calculated according to the Eq. (5).

$$NR = \frac{OR}{CS} \tag{5}$$

where OR and NR represented the original results and normalized results of environmental impacts of WNB, respectively, and CS represented the compressive strength of WNB after corresponding curing ages. The normalized results are shown in Fig. S6. The reduction in environmental

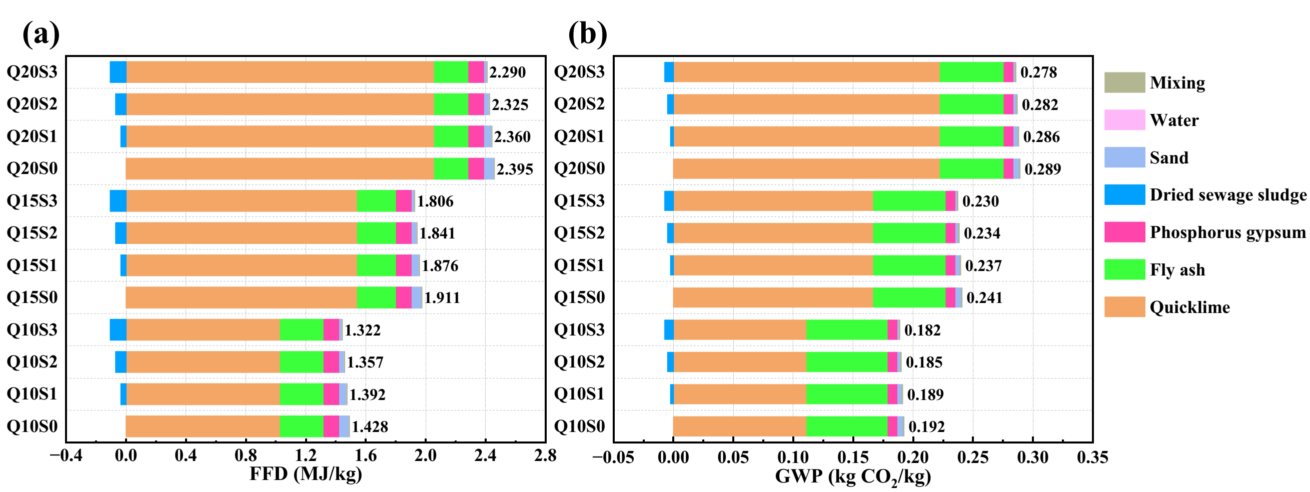

Fig. 7 Environmental impacts of WNB with various sewage sludge content

impacts of WNB was at the cost of a decrease in its compressive strength. The normalized results of FFD and GWP showed a slight increase with the additional level of SS. Furthermore, the normalized results of WNB after 3 days of curing were higher than after 1-day curing. This was attributed to the fact that random internal defects could be generated in WNB specimens after long-term high-temperature curing (Xiang et al. 2021). The values of AP and POCP decreased significantly with the increase in the additional level of SS. This was consistent with the original results of LCA. Interestingly, at the 10% dosage level of quicklime, the normalized results (3 days) of FFD and GWP with 30% SS incorporation were lower than those with 20% SS incorporation. This revealed that a higher dosage of SS may not necessarily lead to an increase in normalized results.

To present a more comprehensive comparison of the environmental advantages of WNB, the environmental impacts of traditional clay bricks were also collected to compare with Q15S3 samples (Fig. 8). Compared to traditional clay bricks, the environmental impacts of WNB were significantly lower. The FFD value of Q15S3 was only half that of clay bricks, and the GWP value of Q15S3 decreased by one-third compared to traditional clay bricks. Besides, the AP and POCP values of Q15S3 even turned negative due to reduced environmental impacts by avoiding landfilled sewage sludge (Septien et al. 2020). The WNB has the potential to replace traditional clay bricks as a new building material, which could avoid the carbon emissions generated by traditional clay brick firing and the consumption of non-renewable resources. Besides, the development of WNB provides a feasible solution for the resource utilization of industrial solid waste.

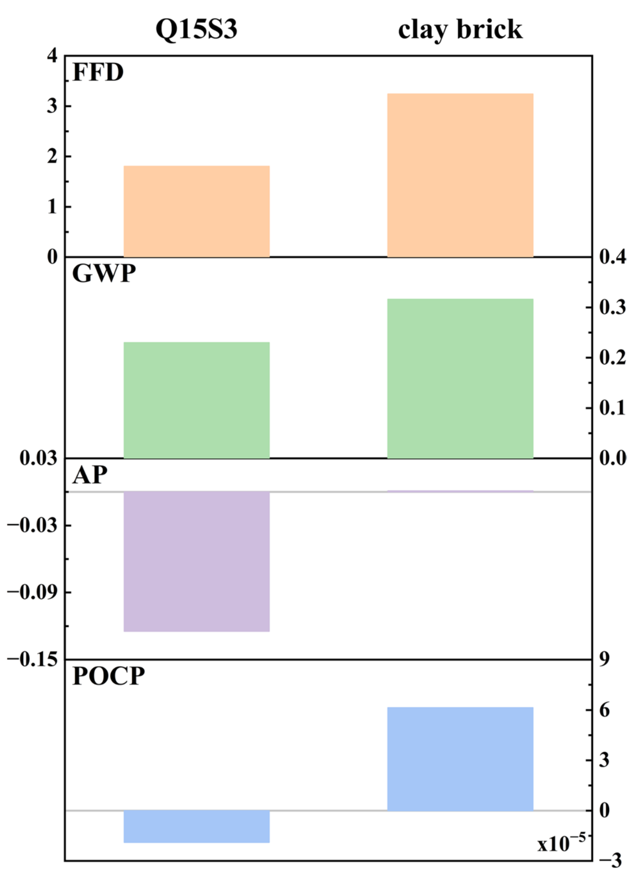

Fig. 8 Comparison between developed non-sintered bricks and traditional clay bricks

Conclusions

This study aimed to investigate the synergy effect of multiple industrial solid wastes in non-sintered bricks and designed an eco-friendly WNB as a substitution for traditional clay bricks. The key findings of this research were as follows:

1. The compressive strength of WNB met the A5 grade of building materials, demonstrating its potential as a viable construction material.
2. Sludge incorporation increases the proportion of large pores within the WNB matrix, resulting in a weaker microstructure. Additionally, harmful elements in the sludge inhibit the formation of C-S–H gels, further compromising the mechanical properties.
3. The leaching behavior results demonstrated that PTEs present in SS were effectively immobilized in WNB specimens, ensuring compliance with environmental safety requirements.
4. Compared to traditional clay bricks, the manufacture of WNB reduced nearly 45% in energy consumption and 17% in CO_2 emissions, highlighting its environmental benefits.

Overall, WNB showed excellent promise as a substitution for traditional clay bricks, offering a sustainable and eco-friendly solution for the construction industry. Future research will focus on further enhancing the durability and mechanical properties of WNB to ensure its long-term viability and performance.

Supplementary Information The online version contains supplementary material available at https://doi.org/10.1007/s11356-024-34559-1.

Author contribution Daquan Shi: conceptualization, methodology, data curation, investigation, writing—original draft preparation.
Xiaobing Ma: methodology, data curation, investigation.
Yading Zhao: conceptualization, methodology, investigation, supervision, validation, project administration, resources, funding acquisition, writing—review and editing.
Jian Wang: methodology, data curation, investigation.
Yan Xia: conceptualization, methodology, data curation, investigation, writing—review and editing.
Minghao Liu: methodology, data curation, writing—review and editing.

Funding The authors sincerely acknowledge the financial support from the National Natural Science Foundation of China (Grant No. 523B2065).

Data availability Data associated with the study has not been deposited into a publicly available repository and data will be made available on request.

Declarations

Ethical approval Not applicable.

Consent to participate All authors participated in the writing of the paper.

Consent for publication All authors agree to publish the paper.

Conflict of interest The authors declare no competing interests.

References

Baeza F, Paya J, Galao O, Saval JM, Garces P (2014) Blending of industrial waste from different sources as partial substitution of Portland cement in pastes and mortars. Constr Build Mater 66:645–653

Balendran RV, Martin-Buades WH (2000) The influence of high temperature curing on the compressive, tensile and flexural strength of pulverized fuel ash concrete. Build Environ 35:415–423

Capony A, Muresan B, Dauvergne M, Auriol JC, Ferber V, Jullien A (2013) Monitoring and environmental modeling of earthwork impacts: a road construction case study. Resour Conserv Recycl 74:124–133

Chen RQ, Ma XQ, Yu ZS, Chen LM, Chen XF, Qin Z (2021) Study on synchronous immobilization technology of heavy metals and hydrolyzed nitrogen during pyrolysis of sewage sludge. J Environ Chem Eng 9(5):106079

Chen T-A (2021) Mechanical properties of glass-based geopolymers affected by activator and curing conditions under optimal aging conditions. Crystals 11(5):502

Cheng JX, Shao ZS, Xu T, Wei W, Qiao RJ, Yuan Y (2021) Experimental research on sintering construction spoil bricks based on microwave heating technology. Environ Sci Pollut Res 28:69367–69380

Chikouche MA, Ghorbel E, Bibi M (2016) The possibility of using dredging sludge in manufacturing cements: optimization of heat treatment cycle and ratio replacement. Constr Build Mater 106:330–341

Cuenca-Moyano GM, Martín-Morales M, Bonoli A, Valverde-Palacios I (2019) Environmental assessment of masonry mortars made with natural and recycled aggregates. Int J Life Cycle Assess 24:191–210

Cui Y, Wang H, Wang D, Wang Q (2022) Effects of Ca(OH)2 on the early hydration, macro-performance and environmental risks of the calcined phosphogypsum. Constr Build Mater 324:126590

Cwiertniewicz-Wojciechowska M, Cema G, Ziembinska-Buczynska A (2023) Sewage sludge pretreatment: current status and future prospects. Environ Sci Pollut Res 30:88313–88330

Cyr M, Coutand M, Clastres P (2007) Technological and environmental behavior of sewage sludge ash (SSA) in cement-based materials. Cem Concr Res 37:1278–1289

Dang J, Hao L, Xiao J, Ding T (2023) Utilization of excavated soil and sewage sludge for green lightweight aggregate and evaluation of its influence on concrete properties. J Clean Prod 390:136061

Ding W, Chen Q, Sun H, Peng T (2019) Modified mineral carbonation of phosphogypsum for CO2 sequestration. J CO2 Util 34:507–515

Duan Y, Wang Q, Yang Z, Cui X, Liu F, Chen H (2022) Research on the effect of steam curing temperature and duration on the strength of manufactured sand concrete and strength estimation model considering thermal damage. Constr Build Mater 315:125531

Gnisci A (2022) Preliminary characterization of hydraulic components of low-temperature calcined marls from the south of Italy. Cem Concr Res 161:106958

Gupta S, Kua HW (2020) Combination of biochar and silica fume as partial cement replacement in mortar: performance evaluation under normal and elevated temperature. Waste Biomass Valor 11:2807–2824

He H, Wang Y, Wang J, Wang S, Huang R, Zheng L, Ding Y (2023) Comparative study on modifications of pH-adjusted fluorogypsum by potassium carbonate and potassium bicarbonate. Constr Build Mater 376:131069

Hou H, Zhang S, Guo D, Su L, Xu H (2023) Synergetic benefits of pollution and carbon reduction from fly ash resource utilization—based on the life cycle perspective. Sci Total Environ 903:166197

Huang CR, Mohamed BA, Li LY (2023) Comparative life-cycle energy and environmental analysis of sewage sludge and biomass co-pyrolysis for biofuel and biochar production. J Chem Eng 457:141284

Jitchaiyaphum K, Sinsiri T, Jaturapitakkul C, Chindaprasirt P (2013) Cellular lightweight concrete containing high-calcium fly ash and natural zeolite. Int J Miner Metall Mater 20:462–471

Liu M, Xia Y, Zhao Y, Chi X, Du J, Du D, Guo J, Cao Z (2022a) Na2SO4 modified low-carbon cementitious binder containing commercial low-reactivity metakaolin for heavy metal immobilization: mechanism of physical encapsulation and chemical binding. J Build Eng 60:105194

Liu M, Zhao Y, Yu Z, Cao Z (2022b) Binding of Cu(II) and Zn(II) in Portland cement immobilization systems: effect of C-A-S-H composition. Cement Concr Compos 131:104602

Liu R, Xu Y, Song L, Liu S, Liang Z, Zhu D, Dai X (2023) The effect of repeated energy inputs on the release profiles of extracellular organic substances in sewage sludge. Water Res 233:119776

Lu Z-N, Chen H, Hao Y, Wang J, Song X, Mok TM (2017) The dynamic relationship between environmental pollution, economic development and public health: evidence from China. J Clean Prod 166:134–147

Lyu Z, Shen A, Mo S, Chen Z, He Z, Li D, Qin X (2020) Life-cycle crack resistance and micro characteristics of internally cured concrete with superabsorbent polymers. Constr Build Mater 259:119794

Ma X, Shi D, Xia Y, Zhao Y, Liu M, Yang Y (2024) Controllable setting time of alkali-activated materials incorporating sewage sludge ash and GGBS: the role of retarders. Constr Build Mater 412:134857

Ma X, Zhao Y, Liu M, Xia Y, Yang Y (2023) Sodium gluconate as a retarder modified sewage sludge ash-based geopolymers: mechanism and environmental assessment. J Clean Prod 419:138317

Mejdi M, Saillio M, Chaussadent T, Divet L, Tagnit-Hamou A (2020) Hydration mechanisms of sewage sludge ashes used as cement replacement. Cem Concr Res 135:106115

Mendes BC, Pedroti LG, Fontes MPF, Ribeiro JCL, Vieira CMF, Pacheco AA, de Azevedo ARG (2019) Technical and environmental assessment of the incorporation of iron ore tailings in construction clay bricks. Constr Build Mater 227:116669

Mulya KS, Zhou J, Phuang ZX, Laner D, Woon KS (2022) A systematic review of life cycle assessment of solid waste management:

methodological trends and prospects. Sci Total Environ 831:154903

Peng N, Li Y, Liu Z, Liu T, Gai C (2016) Emission, distribution and toxicity of polycyclic aromatic hydrocarbons (PAHs) during municipal solid waste (MSW) and coal co-combustion. Sci Total Environ 565:1201–1207

Proske T, Rezvani M, Palm S, Müller C, Graubner C-A (2018) Concretes made of efficient multi-composite cements with slag and limestone. Cement Concr Compos 89:107–119

Riaz U, Murtaza G, Saifullah FM, Aziz H, Qadir AA, Mehdi SM, Qazi MA (2020) Chemical fractionation and risk assessment of trace elements in sewage sludge generated from various states of Pakistan. Environ Sci Pollut Res 27:39742–39752

Septien S, Mirara SW, Makununika BSN, Singh A, Pocock J, Velkushanova K, Buckley CA (2020) Effect of drying on the physical and chemical properties of faecal sludge for its reuse. J Environ Chem Eng 8:103652

Shaik S, Arumugam C, Shaik SV, Arıcı M, Afzal A, Ma Z (2022) Strategic design of PCM integrated burnt clay bricks: potential for cost-cutting measures for air conditioning and carbon dioxide extenuation. J Clean Prod 375:134077

Shi D, Xia Y, Zhao Y, Ma X, Wang J, Liu M, Yu K (2024a) Evaluation of technical and gamma radiation shielding properties of sustainable ultra-high performance geopolymer concrete. Constr Build Mater 436:137003

Shi D, Xia Y, Zhao Y, Wang J, Ma X, Liu M, Yu K, Zhang J, Tian W (2024b) Valorization of steel slag into sustainable high-performance radiation shielding concrete. J Build Eng 91:109650

Sigua GC, Adjei MB (2005) Cumulative and residual effects of repeated sewage sludge applications: forage productivity and soil quality implications in South Florida, USA. Environ Sci Pollut Res 12:80–88

Wang J, Wang Y, Yu J, Xu L, Li M, Cheng J, Li Z (2022) Effects of sodium sulfate and potassium sulfate on the properties of calcium sulfoaluminate (CSA) cement based grouting materials. Constr Build Mater 353:129045

Wang J, Guo J, Su J, Huang R, Xu L, Chen S, Chen X, Tang H, Wang Y, Xiang D, Wu S (2024a) Improving the bonding performance of new and old cement pastes by high-temperature treatment on the surface of old cement pastes. J Build Eng 90:109482

Wang J, Li X, Hu Y, Li Y, Hu P, Zhao Y (2024b) Physical and high temperature properties of basalt fiber-reinforced geopolymer foam with hollow microspheres. Constr Build Mater 411:134698

Wang J, Shi D, Xia Y, Liu M, Ma X, Yu K, Zhao Y, Zhang J (2024c) Stabilization/solidification of radioactive borate waste via low-carbon limestone calcined clay cement (LC3). J Environ Chem Eng 12:113129

Wang J, Zhao Y, Shi D, Xia Y, Liu M, Ma X, Yu K (2024d) Microstructure and radiation shielding properties of lead-fiber reinforced high-performance concrete. Ceram Int 50:23656–23667

Wang L, Ur Rehman N, Curosu I, Zhu Z, Beigh MAB, Liebscher M, Chen L, Tsang DCW, Hempel S, Mechtcherine V (2021) On the use of limestone calcined clay cement (LC3) in high-strength strain-hardening cement-based composites (HS-SHCC). Cem Concr Res 144:106421

Wang Y, Lu H, Wang J, He H (2020) Effects of highly crystalized nano CSH particles on performances of Portland cement paste and its mechanism. Crystals 10(9):816

Wang Y, Tang H, Su J, He H, Zhao Y, Wang J (2023) Effect of sodium sulfate and gypsum on performances of expansive grouting material with aluminum as expansion agent. Constr Build Mater 394:132212

Wang Y, Tang H, Sun G, Wang J, Yang J, Zhao Y (2024e) Effect of fluorogypsum and KH2PO4 on physical properties and hydration mechanisms of aluminate cement based grouting materials. Constr Build Mater 417:135346

Wu K, Hu Y, Xu LL, Zhang LT, Zhang X, Su YF, Yang ZH (2022a) Recycling of sewage sludge in clay-free thermal insulation brick: assessment of microstructure, performance, and environment impact. Environ Sci Pollut Res 29:89184–89197

Wu Y, Wang X, Kim S, Wang Z, Liu T, Liu Y (2022b) Experimental study of the working property and strength behavior of waste marine clay with high water content modified with quicklime, ground calcium carbonate, and a WXS-II soil stabilizer. Constr Build Mater 360:129622

Xia Y, Liu M, Zhao Y, Ma X (2022) Microstructure of Portland cement blended with high dosage of sewage sludge ash activated by Na2SO4. J Clean Prod 351:131568

Xia Y, Liu M, Zhao Y, Chi X, Guo J, Du D, Du J (2023a) Hydration mechanism and phase assemblage of blended cement with iron-rich sewage sludge ash. J Build Eng 63:105579

Xia Y, Liu M, Zhao Y, Chi X, Lu Z, Tang K, Guo J (2023b) Utilization of sewage sludge ash in ultra-high performance concrete (UHPC): Microstructure and life-cycle assessment. J Environ Manage 326:116690

Xia Y, Liu MH, Zhao YD, Guo JZ, Chi XF, Du JX, Du DH, Shi DQ (2023) Hydration mechanism and environmental impacts of blended cements containing co-combustion ash of sewage sludge and rice husk: compared with blended cements containing sewage sludge ash. Sci Total Environ 864:161116

Xia Y, Shi D, Wang J, Zhao Y, Yu K, Liu Y, Cui H, Wang L (2023d) Value-added recycling of cathode ray tube funnel glass into high-performance radiation shielding concrete. Resour Conserv Recycl 199:107252

Xia Y, Zhao Y, Liu M, Guo J, Du J, Du D (2023e) Hydration mechanism and phase assemblage of ternary blended cements based on sewage sludge ash and limestone: modified by Na2SO4. Constr Build Mater 364:129982

Xia Y, Shi D, Zhao R, Yu K, Liu M, Mei H, Xu L, Zhao Y, Wang L, Yan J (2024) Iron-rich industrial waste enhanced low-carbon radiation shielding functional composites. J Clean Prod 449:141649

Xiang Y, Long G, Xie Y, Zheng K, He Z, Ma K, Zeng X, Wang M (2021) Thermal damage and its controlling methods of high-speed railway steam-cured concrete: a review. Struct Concr 22:E1074–E1092

Xu L, Wang J, Li K, Hao T, Li Z, Li L, Ran B, Du H (2023) New insights on dehydration at elevated temperature and rehydration of GGBS blended cement. Cement Concr Compos 139:105068

Yague A, Valls S, Vazquez E, Albareda F (2005) Durability of concrete with addition of dry sludge from waste water treatment plants. Cem Concr Res 35:1064–1073

Yao T, Wang Y, Zhang W, Li M, Luo S, Qi S (2024) Influence of recycled waste concrete powders on the performances of sulphoaluminate cement. Constr Build Mater 426:136226

Yu K, Jia M, Tian W, Yang Y, Liu Y (2024a) Enhanced thermo-mechanical properties of cementitious composites via red mud-based microencapsulated phase change material: Towards energy conservation in building. Energy 290:130301

Yu K, Liu C, Li L, Tian W, Yang Y, Liu Y (2024b) Carbon-negative heat-stored limestone calcined clay cement mortar containing form-stable phase change materials. J Clean Prod 437:140703

Yuan X, Huang H, Zeng G, Li H, Wang J, Zhou C, Zhu H, Pei X, Liu Z, Liu Z (2011) Total concentrations and chemical speciation of heavy metals in liquefaction residues of sewage sludge. Biores Technol 102:4104–4110

Zhang W, Liu X, Zhang Z (2022a) Mechanical, expansion and rheological properties of circulating fluidized bed fly ash based ecological cement: a critical review. Int J Miner Metall Mater 29:1670–1682

Zhang Y, Maierdan Y, Guo T, Chen B, Fang S, Zhao L (2022b) Biochar as carbon sequestration material combines with sewage sludge incineration ash to prepare lightweight concrete. Constr Build Mater 343:128116

Zhou X, Lai C, Almatrafi E, Liu S, Yan H, Qian S, Li H, Qin L, Yi H, Fu Y, Li L, Zhang M, Xu F, Zeng Z, Zeng G (2023) Unveiling the roles of dissolved organic matters derived from different biochar in biochar/persulfate system: mechanism and toxicity. Sci Total Environ 864:161062

Zhu X, Luan M, Tang D, Yang K, Yang C (2024a) Understanding the setting behaviours of alkali-activated slag from the dissolution-precipitation point of view. Cement Concr Compos 148:105474

Zhu X, Zhang Z, Luan M, Yang K, Li J (2024b) Temperature-sensitively dissolving of GGBS in neutral and alkali media. Constr Build Mater 418:135353